Supporting Information

On the relevance of inhomogeneity in saturated fatty acid compositions for the crystallization kinetics of fat blends

Julia Seilert[1*], *Tim Hoffmann*[1], *Michael Rappolt*[2], *Eckhard Flöter*[1]

[1] *Department of Food Process Engineering, Technische Universität Berlin, Straße des 17. Juni 135, Berlin 10623, Germany.*

[2] *School of Food Science and Nutrition, Food Colloids and Bioprocessing Group, University of Leeds, LS2 9JT, U.K.*

Content:

***Correspondence:** Department of Food Process Engineering, Technische Universität Berlin, Straße des 17. Juni 135, Berlin 10623, Germany; Email: julia.seilert@tu-berlin.de

1. Non-treated time-resolved DSC data of the industrial grade and binary blends

In chapter "3.2 Isothermal crystallization via DSC" the time-resolved DSC signals were discussed. Since most events happened during the switch of cooling phase to isothermal phase, the sample's signal response is superimposed by the device's temperature regulation/response. To combat this, the signal obtained for rapeseed oil – similar sample mass – was subtracted from the sample's DSC signal. The original data are given in **Figure S1** and **Figure S2.**

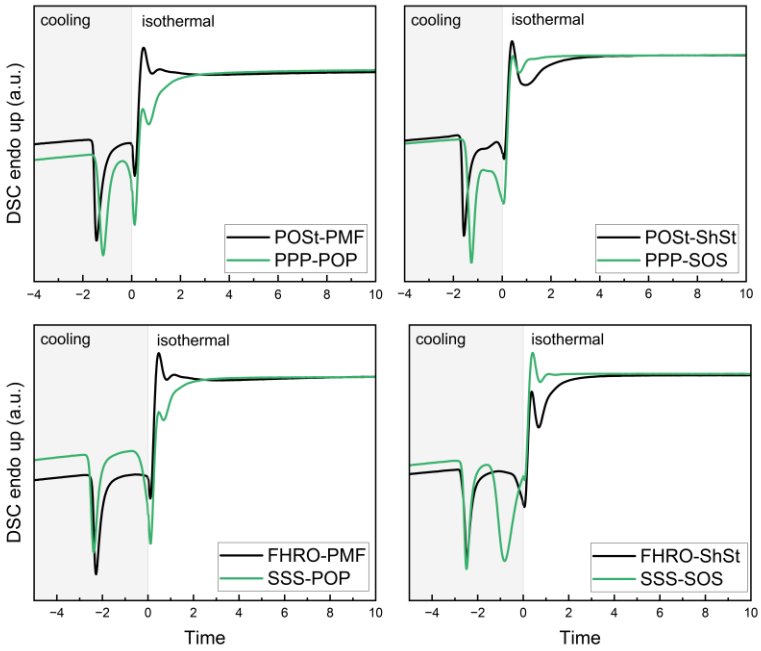

Figure S1. DSC signal obtained during cooling at 10 °C/min and isothermal holding time of 60 min. Time zero is set to the starting point of isothermal phase. Pseudo-binary (black), true-binary (green), material combination as indicated.

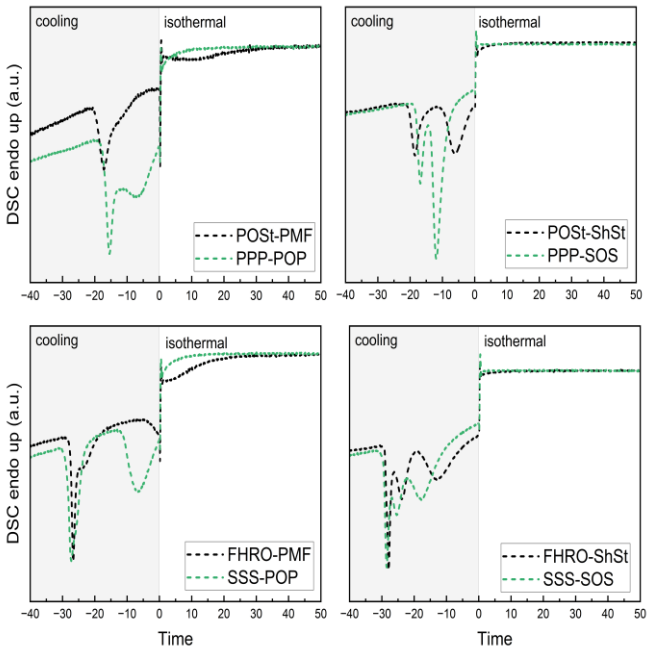

Figure S2. DSC signal obtained during cooling at 1 °C/min and isothermal holding time of 60 min. Time zero is set to the starting point of isothermal phase. Pseudo-binary (black), true-binary (green), material combination as indicated.

2. SAXD/WAXD pattern after liquid subtraction

Note, all data were processed after subtracting the liquid phase. The pattern used for the liquid phase was taken from POSt-ShSt crystallized at 10 °C/min to 5 °C as the temperature is very close to the crystallization temperature 0 °C and no crystalline reflection was determined. Note, to reach an effective cooling rate of 10 °C/min a lower exposure time of 10 sec was applied that naturally introduces more noise which also is noticeable after subtracting the liquid phase.

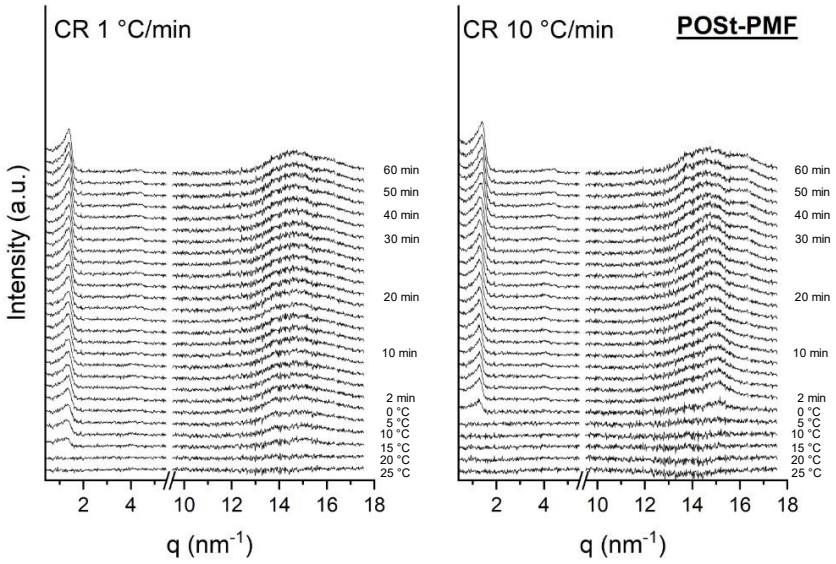

Figure S3. SAXD and WAXD patterns after subtraction of the liquid contribution (obtained at 5 °C for POSt-ShSt cooled at 10 °C/min) of POSt-PMF during cooling at 1 °C/min (left) and 10 °C/min (right) to 0 °C and subsequent isothermal holding time of 60 min. CR = cooling rate.

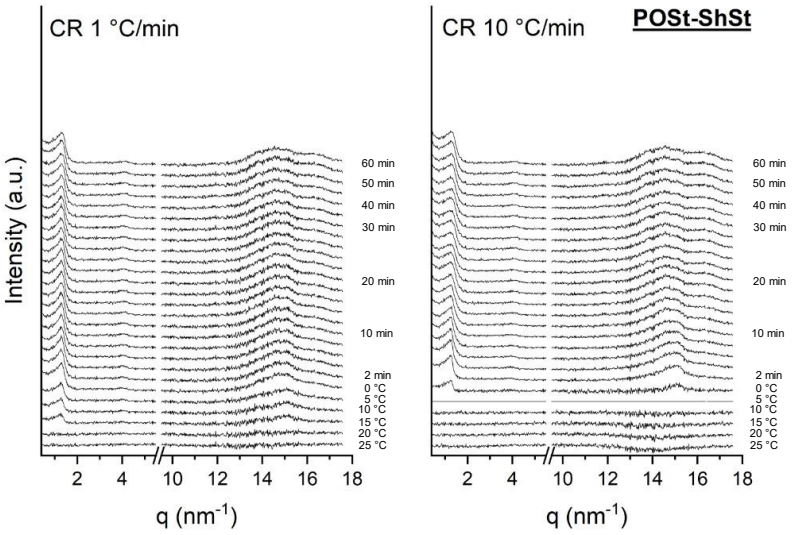

Figure S4. SAXD and WAXD patterns after subtraction of the liquid contribution (obtained at 5 °C for POSt-ShSt cooled at 10 °C/min) of POSt-ShSt during cooling at 1 °C/min (left) and 10 °C/min (right) to 0 °C and subsequent isothermal holding time of 60 min. CR = cooling rate.

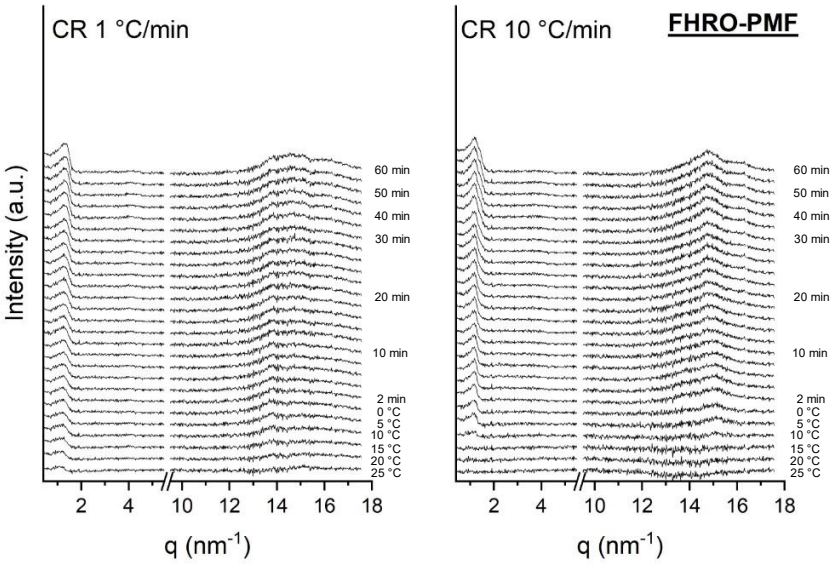

Figure S5. SAXD and WAXD patterns after subtraction of the liquid contribution (obtained at 5 °C for POSt-ShSt cooled at 10 °C/min) of FHRO-PMF during cooling at 1 °C/min (left) and 10 °C/min (right) to 0 °C and subsequent isothermal holding time of 60 min. CR = cooling rate.

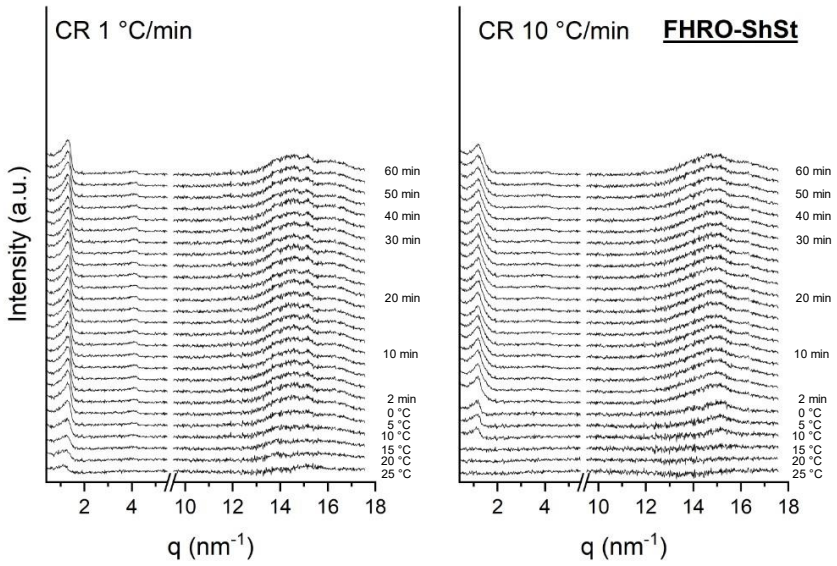

Figure S6. SAXD and WAXD patterns after subtraction of the liquid contribution (obtained at 5 °C for POSt-ShSt cooled at 10 °C/min) of FHRO-ShSt during cooling at 1 °C/min (left) and 10 °C/min (right) to 0 °C and subsequent isothermal holding time of 60 min. CR = cooling rate.

3. WAXS pattern during heating for FHRO-PMF and FHRO-ShSt

Note, no liquid phase was subtracted. The pattern were acquired after cooling the samples at 10 °C/min and an isothermal hold for 60 min at 0 °C. A scan rate of 2 °C/min was applied, allowing to obtained a pattern every 2 °C.

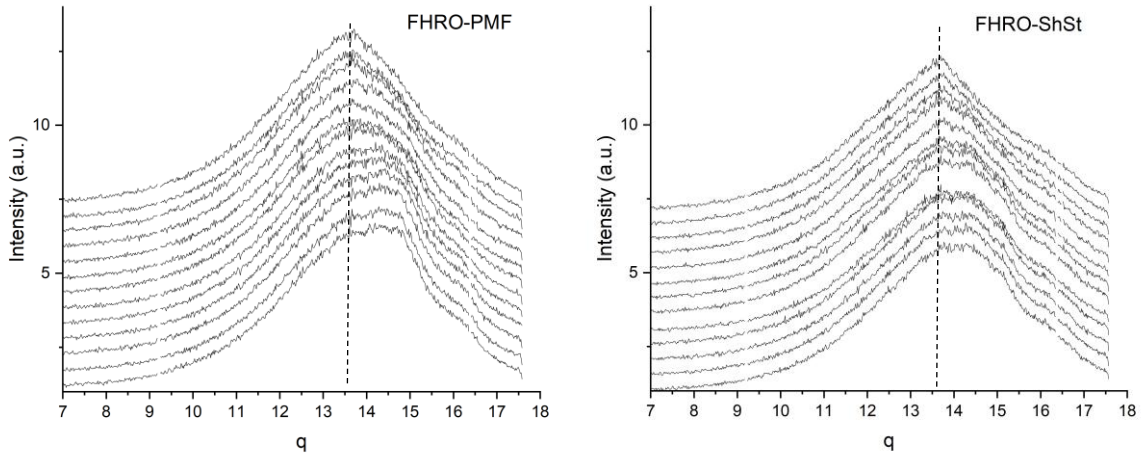

Figure S7. WAXS patterns without liquid subtraction acquired during the heating scan after crystallization (cooling rate of 10 °C/min) of FHRO-PMF and FHRO-ShSt. Depicted are the patterns obtained at 0 °C until 24 °C in 2 °C increments (from bottom to top). Dashed lines indicate the formation of β polymorphs with short spacing of 4.6 Å.

4. Summary of literature data on long and short spacings of pure triglycerides

To identify the polymorphic forms literature data on pure TAGs were used as reference.

Table S1. Long spacings of pure triglycerides in various polymorphs reported in literature, unit Å.

TAG	**α**	**γ**	**β'**	**β**	**Ref.**
PPP	45.6		42.3	40.6	1
SSS	50.6		46.8	45	1
POP	47	75 (3L)	42[a]	61[b] (3L)	2
SOS	49.1 (2L) [c] 54. (3L)[c]	71.8 (3L)	68.9 (3L)	64.5 (3L)	3
PPO	α_2 4.9→4.1[d] (2L) α_1: 76 (3L)		β'_2 :42 (2L) β'_1: 65 (3L)		4
$MC_{POP/PPO}$	46		43-42	42	4

[a] The value relates to β_2' and β_1' with β_1' being more stable than β_2'.
[b] The value relates to β_2.
[c] The value of 49.1 Å refers to α_1-2L and the second value of 54.3 Å refers to the α_2-3L form.
[d] A shifting (001) reflection for α_2-2L was observed during cooling [5].

Table S2. Short spacings of pure triglycerides in various polymorphs reported in literature, unit Å.

TAG	α	γ	β'	β	Ref.
PPP	4.18		4.22, 3.89	$\beta_{1,}$:4.62, 3.9, 3.79 β_2: 4.6, 3.85, 3.7	6
SSS	4.1-4.2		4.2, 3.8	4.6, 3.7, 3.85 β_1: 4.57, 3.84, 3.68 β_2: 4.61, 3.86, 3.70	7 8
POP	4.2	4.8, 4.7, 4.5, 4.0, 3.9 (3L)	β'_2: 4.3 4.2 3.9 β'_1: 4.3, 4.0	β_2: 4.6, 4.1, 3.8, 3.7 (3L)	2
SOS	4.21	4.72, 4.50, 3.88, 3.63 (3L)	4.30, 4.15, 4.02, 3.95, 3.83, 3.70 (3L)	β_2: 4.58, 4.00, 3.90, 3.75, 3.67, 3.57 (3L) β_1: 4.58, 4.02, 3.97, 3.85, 3.80, 3.65 (3L)	9
PPO	4.1 (2L, 3L)		β'_2: 4.2, 3.9 β'_1: 4.2, 3.8 (3L)		4

References

(1) Lutton, E. S. Triple Chain-Length Structures of Saturated Triglycerides. J Am Oil Chem Soc 1948, 70, 248–254.

(2) Bayés-García, L.; Calvet, T.; Àngel Cuevas-Diarte, M.; Ueno, S.; Sato, K. In Situ Observation of Transformation Pathways of Polymorphic Forms of 1,3-Dipalmitoyl-2-Oleoyl Glycerol (POP) Examined with Synchrotron Radiation X-Ray Diffraction and DSC. CrystEngComm 2013, 15 (2), 302–314. https://doi.org/10.1039/C2CE26522B.

(3) Mykhaylyk, O. O.; Hamley, I. W. The Packing of Triacylglycerols from SAXS Measurements: Application to the Structure of 1,3-Distearoyl-2-Oleoyl- Sn -Glycerol Crystal Phases. J. Phys. Chem. B 2004, 108 (23), 8069–8083. https://doi.org/10.1021/jp0379704.

(4) Macridachis, J.; Bayés-García, L.; Calvet, T. Solid Phase Behavior of Mixture Systems Based on Tripalmitoyl Glycerol and Monounsaturated Triacylglycerols Forming a Molecular Compound. Phys Chem Chem Phys 2022, 24 (6), 3749–3760. https://doi.org/10.1039/d1cp05361b.

(5) Macridachis, J.; Bayés-García, L.; Calvet, T. Polymorphic Crystallization and Transformation Pathways of 1,2-Dipalmitoyl-3-Oleoyl-Rac-Glycerol (PPO) during a Liquid–Solid-Liquid Journey. J Therm Anal Calorim 2024. https://doi.org/10.1007/s10973-024-13844-8.

(6) Bhaggan, K.; Smith, K. W.; Blecker, C.; Danthine, S. Binary Mixtures of Tripalmitoylglycerol (PPP) and 1,3-Dipalmitoyl-2-Stearoyl- Sn -Glycerol (PSP): Polymorphism and Kinetic Phase Behavior. Eur. J. Lipid Sci. Technol. 2018, 120 (3), 1700306. https://doi.org/10.1002/ejlt.201700306.

(7) Lavigne, F.; Bourgaux, C.; Ollivon, M. Phase Transitions of Saturated Triglycerides. J. Phys. IV France 1993, 03 (C8), 8-137-8–140. https://doi.org/10.1051/jp4:1993825.

(8) Ghazani, S. M.; Marangoni, A. G. New Triclinic Polymorph of Tristearin. Crystal Growth & Design 2023, 23 (3), 1311–1317. https://doi.org/10.1021/acs.cgd.2c01334.

(9) Sato, K.; Arishima, T.; Wang, Z. H.; Ojima, K.; Sagi, N.; Mori, H. Polymorphism of POP and SOS. I. Occurrence and Polymorphic Transformation. J Am Oil Chem Soc 1989, 66 (5), 664–674. https://doi.org/10.1007/BF02669949.